Encapsulation of ZnO particles by metal fluorides: Towards an application as transparent insulating coatings for windows

Isabelle Trenque, Stéphane Mornet, Etienne Duguet, Jérôme Majimel, Annelise Brüll, Katharina Teinz, Erhard Kemnitz, Manuel Gaudon

Encapsulation of ZnO particles by metal fluorides: Towards an application as transparent insulating coatings for windows

Isabelle Trenque [a], Stéphane Mornet [a], Etienne Duguet [a], Jérôme Majimel [a], Annelise Brüll [a], Katharina Teinz [b], Erhard Kemnitz [b], Manuel Gaudon [a,*]

[a] CNRS, Univ. Bordeaux, ICMCB, 33600 Pessac, France
[b] Institute of Chemistry, Humboldt University Berlin, Brook-Taylor-Street 2, 12489 Berlin, Germany

A B S T R A C T

Because ZnO is a promising candidate for getting efficient films or varnishes with thermal insulating abilities for windows applications, the effect of the encapsulation of ZnO particles in shells of low refractive index material on the improvement of the visible light transmission was investigated. ZnO–MgF_2 core–shell particles were synthesized by deposition of fluoride sols on ZnO particles through a vacuum slip casting process like. The transmission behaviours were first indirectly studied by diffuse reflexion measurements on powder beds. Then, particle films were elaborated by a screen printing process which ensured direct transmission measurements. The encapsulation of ZnO particles with a coating shell of 1.3 wt.% of MgF_2 improves the visible light transmission of 32%.

1. Introduction

Thermal insulating coatings for windows, which are able to limit thermal infrared transmission whereas visible transmittance remains high, are of great interest in building insulation because they are expected to decrease considerably the use of air conditioners and/or heating systems. Transparent conducting oxides (TCOs) have been already used to make infrared-reflective films because their wide bandgap is ideal for optical transmission in the visible range and a nearly total absorption in the UV range [1–6]. Moreover the doping of these metal oxides with *p*-type donors (as example for ZnO matrix: cation Cu^+, anion N^{3-}) or *n*-type donors (in ZnO matrix: cations Al^{3+}, Ga^{3+}, In^{3+} or Si^{4+}, anion F^-) ensures a plasma absorption in the infrared range [7]. TCOs thin films can hence be considered as selective visible light filters. At the present time, these films are produced by physical processes, e.g. magnetron sputtering, CVD, spin coating and dip coating, but these techniques are expensive and complicated to extend on large surfaces and at industrial scale. An alternative approach consists in the application of varnish or the laying of polymeric films where would be dispersed particles transparent in the visible range and absorbing/diffusing in the infrared one. On the contrary to TCO reflector films, these polymeric sheets have to be deposited on the exterior side of the windows in order that the emission of the inorganic particles consecutive to the IR absorption (see Kirchhoff's law) is mainly reemitted by convection outside buildings. The chemical composition of the powders would be advantageously similar to those of conventional TCOs since the *k* extinction coefficient is also directly linked to plasma frequency. Doping ZnO oxide matrix with *n*-type donors (Al, Ga, In, F) is the most developed route to produce heat mirrors [8–14]. Our own recent results demonstrated that aluminium- or gallium-doped ZnO are promising candidates for getting efficient infrared absorbing powders [15,16]. Nevertheless, the refractive index of ZnO ($n = 2.00$) remains too high for ensuring a sufficient transmission of the visible light through the envisaged films/varnishes systems. The encapsulation of ZnO particles with an inorganic shell with a halfway refractive index should improve the visible light transmission. For that purpose, metal fluorides should be promising candidates. The weak polarisability of this class of material ensures low refractive indexes [17]. For instance, magnesium fluoride and zinc fluoride are of particular interest with a refractive index of 1.38 and 1.51, respectively [18]. Notice that MgF_2 is commonly used as antireflective thin films on glasses [19–23]. Here, the fluorides shells deposited on each individual oxide grains act as "anti-diffusive" coatings.

That is why we investigated the preparation and characterization of ZnO–MgF_2 and ZnO–ZnF_2 core–shell particles. Metal fluoride shells were prepared from sols deposited via a vacuum slip casting process like, i.e. from the sol filtration through a ZnO powder bed followed by an annealing stage. Chemical, structural and

* Corresponding author. Address: ICMCB/CNRS, 87 Avenue du Dr. Albert Schweitzer, F-33608 Pessac Cedex, France.
E-mail address: gaudon@icmcb-bordeaux.cnrs.fr (M. Gaudon).

morphological characterizations were performed by Inductively Coupled Plasma Spectrometer (ICP), elemental analysis, X-ray diffraction (XRD) and Transmission Electron Microscopy (TEM). The optical properties were evaluated according to two methods. In a first set of experiments, an indirect estimation of the transmission ability of the core–shell particles was established by diffuse reflectance measurements in mixtures with a black powder. Then, direct transmission measurements were performed through particles films elaborated by a screen printing process.

2. Materials and method

2.1. Preparation of ZnO–MgF_2 and ZnO–ZnF_2 particles

MgF_2 and ZnF_2 sols (0.4 M) were synthesized at room temperature by a non-aqueous method according to previously reported protocols [24,25]. Typically, the synthesis of metal fluoride sols consisted in the dissolution of metal precursors in methanol (dried over $Mg(OCH_3)_2$). For ZnF_2 sol preparation, zinc acetate dehydrate (Aldrich, 99.99%) was used directly as received, whereas in the case of MgF_2 sol, the dimethoxymagnesium precursor was prepared *in situ* by reacting Mg (Aldrich, 99.90%) in methanol. The fluorination was carried out under vigorous stirring by adding the stoichiometric amount of HF solution prepared from the saturation of anhydrous methanol by HF gas flux (Solvay Fluor Hannover, 99.80%); the concentration of HF (12.9 M) was calculated from the relative weight increase of the solution after its saturation.

The ZnO-based core–shell particles were obtained by a vacuum slip casting process (Fig. 1). It was selected according to the fact that a liquid coats a substrate as soon as a critical speed of coating (flow speed of the liquid through the particles bed) is reached [26]. Five grams of ZnO particles (Alfa Aesar, particles diameter: 40–100 nm) were first introduced in a Schlenk filter and dried under vacuum. Ten millilitre of metal fluoride sol (0.4 M) were added under inert atmosphere and soaked for 5 min. Then, the dispersion was filtrated under argon atmosphere. The metal fluoride shell was crystallised by annealing under argon atmosphere in an oven at various temperatures (200 °C, 350 °C or 500 °C).

2.2. Characterization of ZnO–MgF_2 and ZnO–ZnF_2 particles

Chemical compositions were determined by CHNS analyser, for the carbon and hydrogen content, and by the ICP method in order to extract the Zn/Mg ratio for the ZnO–MgF_2 particles. C, H, N, S microanalysis was performed by the Pregl–Dumas method on a ThermoFischer Flash EA1112 and ICP method was performed on a Varian 720ES.

The morphology was investigated by TEM and high resolution TEM (HRTEM) on JEOL 2200 FS equipped with a field emissive gun, operating at 200 kV and with a point resolution of 0.23 nm. Chemical analysis carried out by STEM (Scanning Transmission Electron Microscope) coupled to EDX (Energy Dispersive X-ray spectroscopy) were also acquired with this apparatus.

XRD measurements were carried out at room temperature in the $10° \leqslant 2\theta \leqslant 80°$ range (step 0.017°) on a PANalytical X'PERT PRO diffractometer equipped with X'Celerator detector mounted in Bragg–Brentano scattering geometry. Cu Kα ($K\alpha_1 - K\alpha_2$) radiation was used as X-ray source.

2.3. Diffuse reflectivity measurements

Diffuse reflectance spectra $R(\lambda)$ were recorded at room temperature from 350 to 850 nm with a step of 1 nm and a bandwidth of 2 nm on a Cary 17 spectrophotometer using an integration sphere. Halon (polytetrafluoroethylene) was used as white reference for the blank due to its highly Lambertian diffuse reflectance (superior to 94%) in whole the 250 nm to 2500 nm range. Diffuse reflectance measurements were made on mixtures of different white powders (commercial ZnO, synthesized ZnO-based core–shell and MgF_2 powders) with a black powder Co_3O_4 (Alfa Aesar, 99.7%). The reflectivity spectra are then transformed in Kubelka–Munk (K/S) spectra.

2.4. Direct transmission through films of particles

Ethylcellulose (3 wt.%) was dissolved in terpineol (71 wt.%) to get an agglomerate-free highly viscous solution and ZnO-based particles (26 wt.%) were next dispersed into the mixture basing on previous studies [27]. The paste obtained was deposited onto glass substrates using a screen printing machine (AUREL Model C890). Then, the films were dried under oven at 80 °C. The thickness and the surface profile of the film were measured using an optical profilometer (WYKO NT1100).

Direct transmission spectra $T(\lambda)$ were recorded at room temperature from 300 to 1000 nm (Cary 17 spectrophotometer). A film obtained from a mixture of ethylcellulose (4 wt.%) and terpineol (96 wt.%) coated on a glass substrate was used as blank reference.

3. Results and discussion

3.1. Core–shell particles synthesis and characterization

The chemical composition of ZnO-based core–shell particles was first determined in terms of carbon residues and studied as a function of the annealing temperature (Table 1). It shows carbon residues remained in ZnO–ZnF_2 particles, whereas they are in negligible concentration in any ZnO–MgF_2 sample. This difference was attributed to the fact that precursors are metal alkoxide on one side and metal acetate on the other side. It seems that the use of a magnesium algreene as Mg source allows a complete fluoro-condensation reaction whereas the fluoro-condensation is not

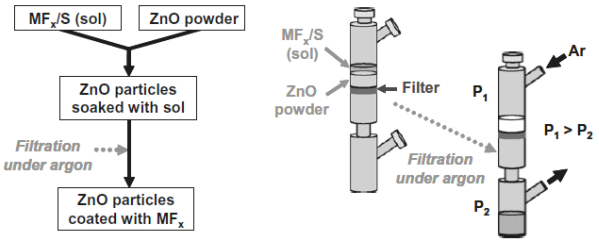

Fig. 1. Schematic representation of the encapsulation process of ZnO particles by metal fluoride. In this figure, *S* refers to the solvent: methanol for MgF_2, methanol with few traces of water for ZnF_2. P_1 and P_2 refer to internal pressures in the top-part and the bottom-part of the Schlenk filter.

Table 1
Carbon weight ratio in ZnO particles coated with metal fluoride as a function of the annealing temperature (4 h in argon atmosphere).

	200 °C/Ar	350 °C/Ar	500 °C/Ar
Carbon weight ratio in sample coated with ZnF_2	0.158(2)	0.17(2)	0.128(7)
Carbon weight ratio in sample coated with MgF_2	0.084(8)	0.054(7)	0.06(2)

complete for ZnF_2 sol from the use of zinc acetate. Moreover, for the ZnO–ZnF_2 particles for whose carbon residues were in non negligible concentration, it can be seen the carbon weight ratio decreased with the increase of the annealing temperature. This data is in good agreement with the fact that non-structured carbon impurities are easily removed with a moderate annealing.

TEM images and chemical cartographies obtained with coupled EDX analyses first confirmed the presence of MgF_2 as continuous shell on ZnO particles (Fig. 2). However, in the case of ZnO–ZnF_2 particles, the comparison of STEM images and STEM EDX maps revealed that the ZnF_2 compound was present but not as a coating onto the ZnO cores, but as core-free particles. A mixture of ZnO particles and ZnF_2 particles was obtained. This diverging behaviour could be due to differences in the wettability behaviour of ZnO cores with regards to ZnF_2 and MgF_2 sol dispersions. In both cases, the solvent used was anhydrous methanol but for the ZnF_2 sol preparation, some water traces provided by the zinc acetate dehydrate used as zinc precursor may increase the sol surface tension (water surface tension is significantly higher than methanol surface tension: 72.7 mJ m^{-2} and 22.7 mJ m^{-2}, respectively). Thus, the coating of the ZnO powder seems very sensitive to the sol surface tension, however, a sol with a very low surface tension is required in order to obtain suitable coating process.

XRD analysis of raw and post-annealed ZnO–MgF_2 particles showed characteristic wurtzite ZnO diffraction peaks in the powder diffractograms (Fig. 3). Considering the main peak of the MgF_2 rutile phase (1 1 0 peak), an increase of its relative intensity with the annealing temperature was observed, associated to a decrease of the full width at half maximum (Fig. 3, right column). This observation shows that the annealing treatment is necessary for the MgF_2 shell crystallisation.

3.2. Optical properties

3.2.1. Theoretical section

Many models describe light-matter interactions. Unfortunately, in the various models used to describe the interactions between light and a theoretical interface, e.g. through a film or on an opaque powder bed, the geometrical light partition is described in different ways.

In the scope of the two-flux method, a front and a back flux (i.e. transmitted flux and reflected flux, respectively) on an interface, the Fresnels model with the Fresnel's transmission (T_F) and reflectance coefficients (R_F) [28] is the more appropriate. By considering an interface between a material of refractive index n_1 and the environment of n_2 under normal incidence and without absorption phenomena, the Fresnel transmission coefficients are given by the following equation

$$R_F + T_F = 1 \tag{1}$$

$$R_F = \frac{(n_1 - n_2)^2}{(n_1 + n_2)^2} \tag{2}$$

This model predicts the improvement of T_F through ZnO particles in the visible range while these particles are encapsulated by MgF_2 shells. In the case of core–shell particles, T_F was calculated, in a first approximation, as the sum of the transmission at the core/shell interface and at the shell/matrix interface. The development of the previous Eqs. (1) and (2) on a single ZnO particle and a ZnO–MgF_2 particle is illustrated in Fig. 4. The calculation confirmed an increase of T_F while the shell refractive index is halfway between the core and the environment ones. For instance, the comparison of T_F values for a simple ZnO/air interface ($n_{ZnO} = n_1 = 2$ and $n_{air} = n_2 = 1$) and for a double ZnO/MgF_2/air interface ($n_{MgF2} = n_3 = 1.37$) showed a T_F increase from 89% to 94%. In the case of dispersions, the Fresnel transmission coefficient of the material ($T_{Fmaterial}$) depends not only on that of the dispersed objects ($T_{Fobject}$), but also on the number of objects ($N_{objects}$) crossed by the incident light as shown in the following equation

$$T_{F_{material}} = (T_{F_{object}})^{N_{objects}} \text{ and then,}$$
$$N_{objects} = \log(T_{F_{material}}) / \log(T_{F_{object}}) \tag{3}$$

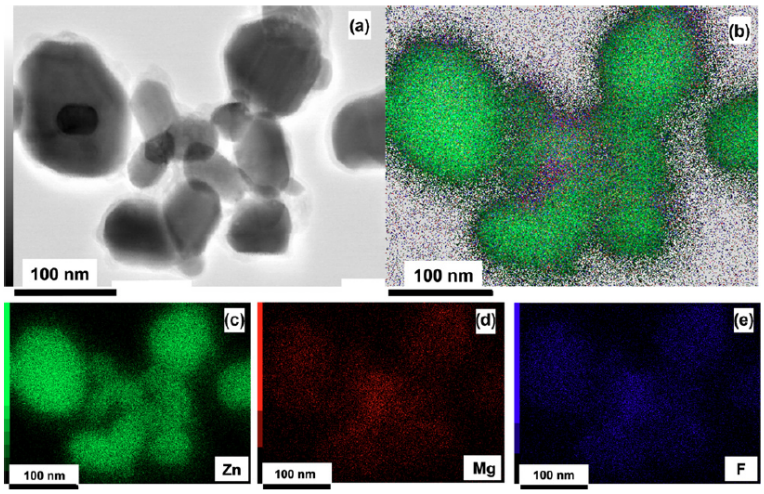

Fig. 2. (a) STEM image of a ZnO–MgF_2 sample, (b) STEM EDX mapping with Zn, Mg and F signals, (c–e) STEM EDX mappings of Zn, Mg and F, respectively.

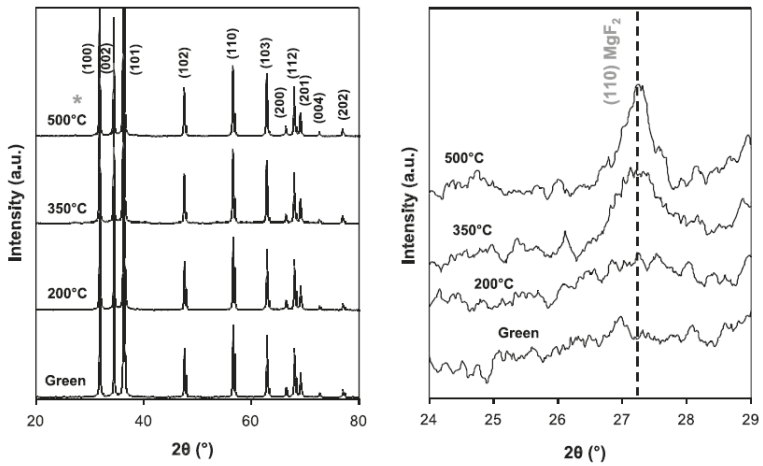

Fig. 3. X-ray diffraction patterns of green ZnO–MgF_2 particles and the same particles annealed at different temperatures (4 h in argon atmosphere). The X-ray diffraction patterns are indexed to the diffraction of wurtzite ZnO (on the left figure). Intensity of the strongest peak of rutile MgF_2 with treatment of calcination is magnified on the right figure.

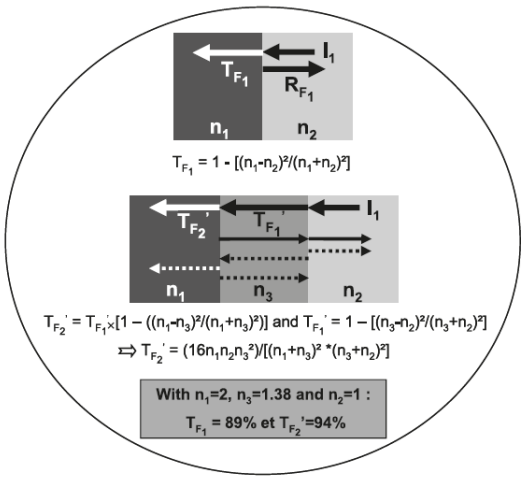

Fig. 4. Comparison of the visible light transmission between a simple interface ($n_1 - n_2$) and a double interface ($n_1 - n_2$) with a halfway n_3 refractive index.

As $2\log(0.94) \approx \log(0.89)$, a similar transparency (i.e. similar $T_{Fmaterial}$ values) was expected for a ZnO–MgF_2 particle concentration twice that of the ZnO single particle concentration. This result confirmed the interest of using core–shell particles.

In another descriptive model, the transmission can be described as front scattering (T) and reflection as back scattering (R). Materials are then characterized by their transmittance and reflectance factors *vs.* absorption and scattering coefficients (K and S, respectively) [28]. In a first approximation whatever the K value is, it can be predicted that R would increase and T would decrease while the powder S value increases.

In the case of dispersed particles into a polymeric matrix, the light transmission through such a polymeric sheet is not only dependent on the absorption and the scattering coefficients of the dispersed and dispersing materials, but would also depend on the particles concentration and their dispersion optimization (absence of agglomerates, etc.), as illustrated in Fig. 5a for a film made of a polymeric matrix in which ZnO particles would be dispersed. A first solution is to study powder mixtures in order to be not perturbed by extrinsic parameters. Hence the effect of encapsulation of ZnO by MgF_2 shell was indirectly studied by scattering measurements on opaque powder film, i.e. sufficiently thick to ensure a null transmission ($T = 0$). The K and S coefficients were easily extracted from scattering reflectivity measurements on opaque powder bed. According to the Kubelka & Munk laws [28–30], the K and S coefficients are extractable from Eq. (4) by determination of the reflectance factor (ρ) of the powder (evaluated by the scattering measurements).

$$\frac{K}{S} = \frac{(1-\rho)^2}{2\rho} \tag{4}$$

The problem raised by the use of powders with absorption coefficients nearly equal to zero, such as ZnO and ZnO–MgF_2 powders, is that a modification of the diffusion coefficient does not imply a change in the reflectance factor (ρ is always equal to 1). Thus, Eq. (4) was not sufficient to characterize the encapsulation effect. Another relation (Eq. (5)), inspired from Eq. (4) and considering the Duncan laws for a mixture of two powders (with absorption and diffusion coefficients equal to K_a, S_a and K_b, S_b, respectively), has to be used

$$\left(\frac{K}{S}\right)_m = \frac{C \cdot K_a + (1-C) \cdot K_b}{C \cdot S_a + (1-C) \cdot S_b} \tag{5}$$

In this formula, K and S are the absorption and diffusion coefficients of the mixture and C is the weight ratio of the first powder inside the mixture. By considering a mixture of a transparent powder ($K_a = 0$) and absorbent powder ($K_b \neq 0$), Eq. (5) becomes

$$\left(\frac{K}{S}\right)_m = \frac{(1-C) \cdot K_b}{C \cdot S_a + (1-C) \cdot S_b} \tag{6}$$

and then, $$\left(\frac{K}{S}\right)_m = \frac{(1-C) \cdot (K_b/S_b)}{C \cdot (S_a/S_b) + (1-C)} \tag{7}$$

After the determination of the K/S ratio of various powder mixtures and the K_b/S_b powder ratio, the plotting of the K/S ratio *vs.* C gave the

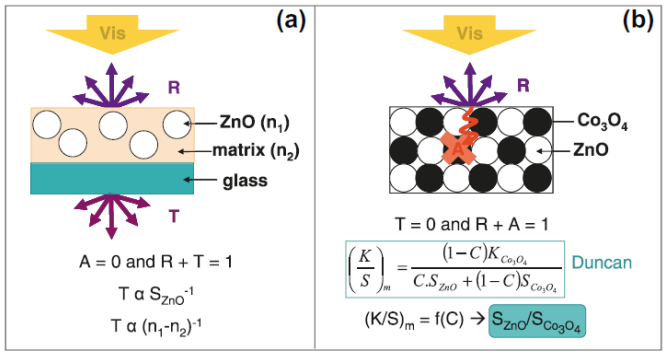

Fig. 5. Process for optical properties characterization. Optical effects when measuring the transmission through a polymeric film in which ZnO particles are dispersed (on the left figure). Optical effects when measuring the diffuse reflexion on a bed powder of a mixture of ZnO and Co_3O_4 powders (on the right figure).

S_a/S_b ratio, as illustrated in Fig. 5b in the case of a mixture of ZnO with a standard "black" Co_3O_4 powder. The same reasoning was reproduced for a mixture of the ZnO–MgF_2 particles ($K_{ZnO-MgF2} = 0$) with the same Co_3O_4 powder. The $S_{ZnO}/S_{Co_3O_4}$ and $S_{ZnO-MgF2}/S_{Co_3O_4}$ values allowed the comparison of S_{ZnO} and $S_{ZnO-MgF2}$. Then, the effect of the encapsulation of the ZnO particles on the visible light transmission can be qualitatively evaluated.

3.2.2. Results

The visible light transmission of ZnO, MgF_2 and ZnO–MgF_2 "white powders" ($K = 0$) was studied by scattering reflexion measurements. The experiments were made on the pristine ZnO particles, post-annealed ones at 200 °C MgF_2 and ZnO–MgF_2 particles, this post annealing temperature being the best compromise to initiate crystallisation of MgF_2 (i.e. evaporation of all the organics) without inducing a partial substitution of oxygen for fluorine.

The K/S ratios of mixtures of each powder with the standard "black" Co_3O_4 powder (ZnO/Co_3O_4, MgF_2/Co_3O_4 and ZnO–MgF_2/Co_3O_4 mixtures) were measured for various weight ratios (C) of the "white" powder in the mixture. For illustration, the 50/50 mixture reflective spectra and the K/S Kubelka & Munk spectra are reported for comparison in Fig. 6. An average K/S ratio on the visible range (400–800 nm) was calculated for each mixture for various powder ratios. The K/S ratio evolution *vs.* the white powder weight ratio within the mixture is plotted on Fig. 7. The extracted diffusion coefficients from Eq. (7) ratio between ZnO, MgF_2 and ZnO–MgF_2 particles and the Co_3O_4 powder are listed in Table 2.

$S_{ZnO-MgF2}/S_{Co_3O_4}$ ratio was measured being lower than $S_{ZnO}/S_{Co_3O_4}$ ratio, which implies that the diffusion coefficient of the ZnO–MgF_2 particles was largely lower than the diffusion coefficient of the ZnO particles. To discriminate a coating effect from a simple additive effect (MgF_2 being less diffusive than ZnO), the K/S calculation of additive mixtures of three powders (ZnO, MgF_2, Co_3O_4) with various compositions was carried out. In this model, C' is the weight ratio of the two white powders (i.e. the mixing rate of ZnO and MgF_2 particles). To obtain the same K/S behaviour as in the case of ZnO–MgF_2/Co_3O_4 mixtures, the white powder should be made of 50 wt.% of ZnO and 50 wt.% of MgF_2. ICP measurements shown that the ZnO–MgF_2 particles were made of 1.3 wt.% of MgF_2. The very low S value obtained for ZnO–MgF_2 confirmed the phenomenon was really due to the coating effect and not a mixture effect. It was shown that the encapsulation of ZnO particles by MgF_2 is very efficient to decrease the diffusion coefficient of ZnO particles.

Finally, the transmission properties of ZnO film and ZnO–MgF_2 composite films elaborated by screen printing process were performed. All the films were elaborated in the same experimental conditions. In the case of the ZnO–MgF_2 composite coatings, films from additive mixture of ZnO (98.7 wt.%) and MgF_2 (1.3 wt.%) powders and from ZnO–MgF_2 particles (with same weight ratio) were compared. Film pictures are presented in Fig. 8. The direct transmissions in the visible range (400–800 nm) of the three compared films are reported in Fig. 9. The average transmission was calculated equal to 48% for the ZnO film, 60% for the film made from ZnO and MgF_2 additive mixture and 80% for the latter made from

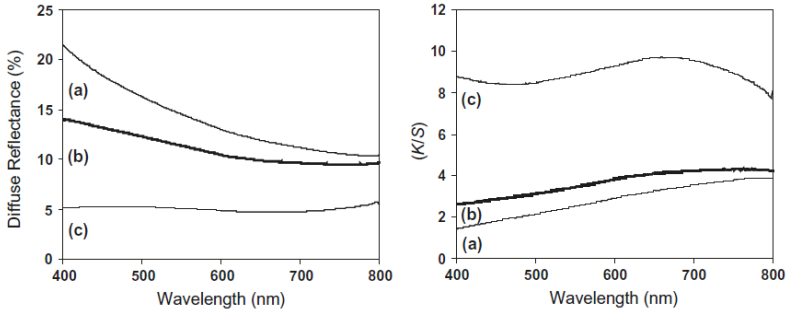

Fig. 6. Diffuse reflectance spectra in the visible range (400–800 nm) and the (K/S) ratios associated for 50/50 mixtures: (a) 50/50 ZnO/CO_3O_4, (b) 50/50 ZnO–MgF_2/CO_3O_4, (c) 50/50 MgF_2.

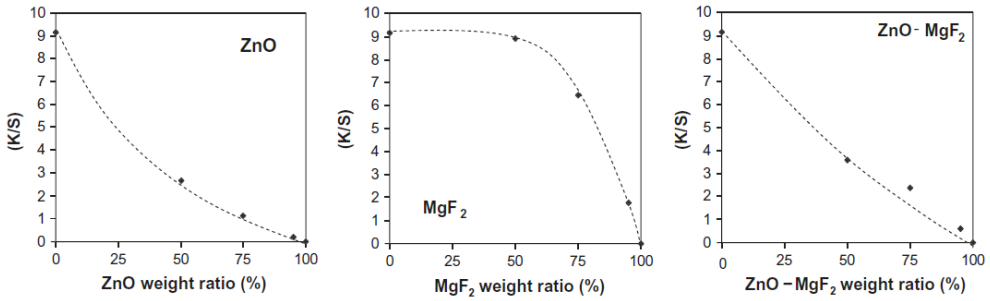

Fig. 7. *K*/*S* ratio within ZnO/Co_3O_4, MgF_2/Co_3O_4 and $ZnO–MgF_2/Co_3O_4$ mixtures as a function of the ZnO, MgF_2 or $ZnO–MgF_2$ weight ratio, respectively. The real values are represented by black dots and the associated models are represented by broken lines. *K*/*S* curves were fitted using Eq. (7).

Table 2
ZnO, MgF_2 and $ZnO–MgF_2$ scattering coefficients relatively given to the scattering coefficient of Co_3O_4.

	ZnO/Co_3O_4	$ZnO@MgF_2/Co_3O_4$	MgF_2/Co_3O_4
$S_{\text{white powder}}/S_{Co_3O_4}$	2.43 ± 0.02	1.30 ± 0.07	0.15 ± 0.03

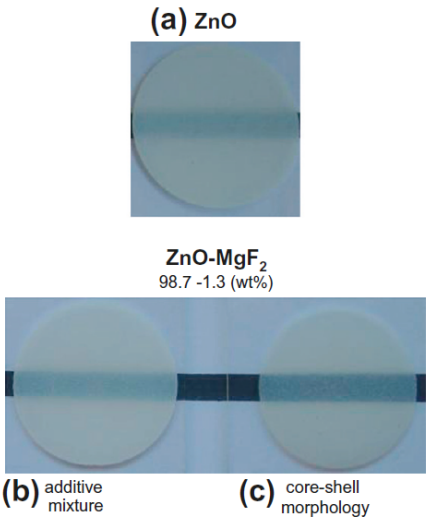

Fig. 8. Pictures of the films elaborated by screen printing process from: (a) ZnO, (b), ZnO (98.7 wt.%)–MgF_2 (1.3 wt.%) additive mixture, (c) $ZnO–MgF_2$ core–shell particles.

$ZnO–MgF_2$ particles. Both film pictures and transmission measurements shown that (i) the ZnO films were largely more opaque than the "mixture" films, (ii) the visible transmission was obviously better for the films based on core–shell particles than for the "mixture" films of similar composition. It has to be noted that for all films, optical profilometer analysis showed inhomogeneous surfaces with a thickness between 3 and 10 μm and a roughness in the micrometer range. Since the morphology of the films are almost similar, it cannot be the source of the differences observed in the transmission behaviours. Consequently, the encapsulation of particles in shells of low refractive index should be an efficient route to improve the visible light transmission of inorganic particles dispersed in a polymeric matrix. Herein, it was shown for ZnO particles that the use as coating shells of 1.3 wt.% of magnesium fluoride allows a drastic improvement of the transmission percentage between the composite sheet and the ZnO one.

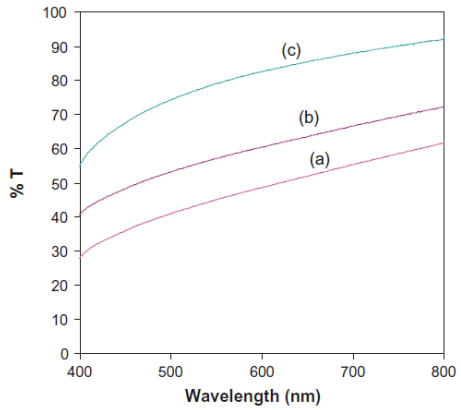

Fig. 9. Transmission spectra in the visible range (400–800 nm) of the films elaborated by screen printing process from: (a) ZnO, (b), ZnO (98.7 wt.%)–MgF_2 (1.3 wt.%) additive mixture, (c) $ZnO–MgF_2$ core–shell particles.

4. Conclusions

For the first time, $ZnO–MgF_2$ particles were synthesized. The synthesis was made by deposition of magnesium fluoride sols on ZnO particles via a vacuum slip casting process like. The crystallisation of the MgF_2 shell was achieved by a further stage of annealing. An annealing at 200 °C is the best compromise to initiate crystallisation of MgF_2 (i.e. evaporation of all the organics) without inducing traces of oxide into the fluorides. The optical properties were studied by two methods: diffuse reflexion measurements on powder beds using the Kubelka & Munk law and direct transmission measurements on films elaborated by screen printing process. In both cases, it was shown that the encapsulation of ZnO particles by MgF_2 is very efficient in order to decrease the light diffusion coefficient of ZnO particles and then, to increase the visible light transmission of the particles. The use of ZnO particles with coating shells of 1.3 wt.% of magnesium fluoride allows an improvement of 32% of the transmission. When considering an additive mixture of 98.7 wt.% ZnO and 1.3 wt.% MgF_2 powders,

the transmission is improved by 12% only. This ensures that the phenomenon was really the consequence of the coating effect and not a mixture effect. Consequently, the strategy using nanostructured materials in core–shell architecture with a shell composed by a low refractive index material seems an interesting route for the improvement of the visible light transmission of films or varnish in which Al-doped ZnO or Ga-doped ZnO transparent and infrared absorbing powder is dispersed for thermal insulating coatings for windows.

References

[1] B. Lewis, D. Paine, MRS Bull. 25 (2000) 22–27.
[2] I. Hamberg, C.G. Granqvist, Sol. Energy Mater. 11 (1984) 239–248.
[3] A. Hjortsberg, I. Hamberg, C.G. Granqvist, Thin Solid Films 90 (1982) 323–326.
[4] R.P. Howson, J.N. Avaritsiotis, M.I. Ridge, C.A. Bishop, Thin Solid Films 63 (1979) 163–167.
[5] C.M. Lampert, Sol. Energy Mater. 6 (1981) 1–41.
[6] T. Coutts, D. Young, X. Li, MRS Bull. 25 (2000) 58–65.
[7] R.G. Gordon, MRS Bull. 25 (2000) 52–57.
[8] D.C. Altamirano-Juarez, G. Torres-Delagado, S. Jimenez-Sandoval, O. Jimenez-Sandoval, R. Castanedo-Perez, Sol. Energy Mater. Sol. Cells 82 (2004) 34–43.
[9] K.Y. Cheong, N. Muti, S.R. Ramanan, Thin Solid Films 410 (2002) 142–146.
[10] Z. Ben Ayadi, L. El Mir, K. Djessas, S. Alaya, Nanotechnology 18 (2007) 445702/1–445702/6.
[11] H. Gomez, A. Maldonado, R. Castanedo-Perez, G. Torres-Delgado, M. de la L. Olvera, Mater. Characteriz. 58 (2007) 708–714.
[12] M. Suguyama, A. Murayama, T. Imao, K. saiki, H. Nakanishi, S.F. Chichibu, Phys. Status Solidi A 203 (2006) 2882–2886.
[13] S. Major, A. Banerjee, K.L. Chopra, Thin Solid Films 122 (1984) 31–43.
[14] W.W. Wenas, A. Yamada, K. Takahashi, M. Yoshino, M. Konogai, J. Appl. Phys. 77 (1991) 107–117.
[15] H. Serier, M. Gaudon, M. Menetrier, Solid State Sci. 11 (2009) 1192–1197.
[16] H. Serier, A. Demourgues, M. Gaudon, Inorg. Chem. 49 (2010) 6853–6858.
[17] J. Lucas, F. Smektala, J. Adam, J. Fluorine Chem. 114 (2002) 113–118.
[18] D. Popov, Crystallogr. Rep. 47 (2002) 829–831.
[19] H. Krüger, E. Kemnitz, A. Hertwig, U. Beck, Thin Solid Films 516 (2008) 4175–4177.
[20] T. Murata, H. Ishizawa, I. Motoyama, A. Tanaka, Appl. Opt. 45 (2006) 1465–1468.
[21] F. Perales, J. Herrero, D. Jaque, C. de las Heras, Opt. Mater. 29 (2007) 783–787.
[22] K. Kawamata, T. Shouzu, N. Mitamura, Vacuum 51 (1998) 559–564.
[23] S.-H. Woo, Y. Park, D.-H. Chang, K. Sobahan, C. Hwangbo, J. Korean Phys. Soc. 51 (2007) 1501–1506.
[24] J. Krishna Murthy, U. Groβ, S. Rüdiger, E. Kemnitz, J. Winfield, J. Solid State Chem. 179 (2006) 739–746.
[25] S. Rüdiger, U. Groβ, E. Kemnitz, J. Fluorine Chem. 128 (2007) 353–368.
[26] C. Williams, M. Daoud (Eds.), La juste argile, EDP Sciences, 1998.
[27] B. Krishnan, V.P.N. Nampoori, Bull. Mater. Sci. 28 (2005) 239–242.
[28] M. Elias, J. Lafait (Eds.), La couleur. Lumière vision et matériaux, Belin, 2006.
[29] R.J.D. Tilley (Ed.), Colour and Optical Properties of Materials An Exploration of the Relationship between Light the Optical Properties of Materials and Colour, Wiley, 2000.
[30] K. Nassau (Ed.), The Physics and Chemistry of Color, The Fifteen Causes of Color, John Wiley & Sons, New York, 2001.